Time Dependent Density Functional Theory of X-ray Absorption Spectroscopy of Alkaline-Earth Oxides

G. Fronzoni,* R. De Francesco, and M. Stener

Dipartimento di Scienze Chimiche, Università di Trieste, Via L. Giorgieri 1, I-34127 Trieste, Italy, and Consorzio Interuniversitario Nazionale per la Scienza e Tecnologia dei Materiali, INSTM, Unità di Trieste, INFM DEMOCRITOS National Simulation Center, Trieste, Italy

Received: February 11, 2005; In Final Form: March 25, 2005

The time dependent density functional theory (TDDFT) has been employed to calculate the X-ray absorption spectra of the alkaline-earth oxides at the metal K and L and oxygen K edges. Cluster models to mimic the bulk are considered, embedded within an array of point charges to simulate the Madelung potential. Comparison with experimental data allows a precise assessment of the performances of the method, which appears competitive and suitable to reproduce the measurements. The configuration mixing explicitly included in the TDDFT scheme appears mandatory for a correct reproduction of the oscillator strength distribution in the metal 2p spectra. The origin of the theoretical spectral features is investigated with the help of the partial density of the virtual states (PDOS) calculated for each core hole considered. The trends of the spectral features along the series are discussed in terms of the nature of the virtual final states and related to the presence of the empty nd orbitals of the metal cations. The trend of the below-edge features in the O1s excitation spectra is discussed in terms of the metal−oxygen bonding interaction.

1. Introduction

It is well established that the X-ray absorption structures near the ionization threshold (NEXAFS region) are closely related to the local electronic structure around the atom in which the excitation takes place and contain the most significant information on the low-lying unoccupied states of the systems. From an experimental point of view, the most recent integration between the electron energy loss techniques (EELS) and the transmission electron microscope (TEM)[1,2] has improved the studies in condensed matter also at the nanoscale level. The EELS structures involve transitions from a core orbital strongly localized on a particular atom to the unoccupied electronic states which lie near the ionization limit of this specific core state and extend over an energy range of about 20−30 eV. The relevant excitation energies give an indication of the ordering of the unoccupied levels, while the associated intensity is related to the electric dipole transition moment between the initial core state and the virtual final state. Therefore, the intensity maps the dipole-allowed atomic site component of the virtual states. The fine structure around the K absorption edge has been extensively studied for structural determination due to the quite simple interpretation of the spectra which are governed by the s → p dipole transitions. Potentially richer are however the L-edge structures, in particular of transition metals, since they are associated with the p → d dipole transitions which directly probe the metal d participation in the virtual orbitals, and therefore details of the d involvement in the bonding.

The interpretation of the EELS experimental data of condensed systems requires first principle calculations, and although many efforts have been spent to reproduce the spectra, a standard and robust method has not yet emerged clearly.[3−10] Recently, the time dependent density functional theory (TDDFT) has been extended to the treatment of the core electron excitations[11,12] and its application to calculate the core excitation spectra of solid MgO using a cluster model to mimic the bulk[13] has been tested. The agreement with the experimental data indicates the reliability of the TDDFT approach also in the case of solid samples which may be twofold. One reason is that a finite cluster model should be advantageous for the calculation of core excitations, since the excited electron is localized near the core hole so the description of a limited region would be sufficient to describe it accurately as compared with the band-structure method unless a sufficiently large supercell is chosen to include core hole effects. The second one is the potentiality of the TDDFT method which formally includes the coupling between the single excited configurations, therefore overcoming the limitations of the single particle approaches in terms of coupling between different configurations, which arise when the core state is degenerate like in 2p orbitals and also degenerate final atomic nd contributions are accessible.

We thought it would be important to verify the capability of the computational strategy employed for MgO, extending the study of core excitations to other members of the series of alkaline-earth oxides. In this work, we apply the TDDFT to the calculations of the core excitation spectra of CaO, SrO, and BaO at the metal K and L and the oxygen K edges and compare them with analogous theoretical results for MgO. This represents the first theoretical study which considers all the possible core edges for the series of alkaline-earth oxides at the same level of accuracy, allowing spectral trends to be analyzed across a number of compounds with the same rocksalt structure. Very interesting is the possibility to correlate the spectral features, in particular at the metal L and oxygen K edges, with the presence of the empty nd orbitals of the metal cations which are expected to decrease in energy upon going from MgO to BaO with a consequent increasing participation in the bonding with the oxygen atom.[14,15]

* Corresponding author. E-mail: fronzoni@univ.trieste.it.

10.1021/jp050755y CCC: $30.25
Published on Web 05/03/2005

2. Theoretical Method

The TDDFT approach for electron excitations and its implementation in the ADF code have been described in detail in the literature,[16,17] so here, we just recall the salient steps and describe the new features. The general problem is cast in the following eigenvalue equation:

$$\mathbf{\Omega F}_i = \omega_i^2 \mathbf{F}_i \tag{1}$$

where $\mathbf{\Omega}$ is a four-index matrix with elements $\Omega_{ia\sigma,jb\tau}$; the indexes consist of products of occupied-virtual (ia and jb) Kohn−Sham (KS) orbitals, while σ and τ refer to the spin variable. The eigenvalues correspond to squared excitation energies, while the oscillator strengths are extracted from the eigenvectors $\mathbf{F}_i$.[16] The $\mathbf{\Omega}$-matrix elements can be expressed in terms of KS eigenvalues ϵ and the coupling matrix $\mathbf{K}$:

$$\Omega_{ia\sigma,jb\tau} = \delta_{\sigma\tau}\delta_{ij}\delta_{ab}(\epsilon_a - \epsilon_i)^2 + 2\sqrt{(\epsilon_a - \epsilon_i)}\sqrt{(\epsilon_b - \epsilon_j)}K_{ia\sigma,jb\tau} \tag{2}$$

The elements of the coupling matrix $\mathbf{K}$ are given by

$$K_{ia\sigma,jb\tau} = \int d\mathbf{r} \int d\mathbf{r}'\, \varphi_{i\sigma}(\mathbf{r})\, \varphi_{a\sigma}(\mathbf{r})\left[\frac{1}{|\mathbf{r}-\mathbf{r}'|} + f_{xc}^{\sigma\tau}(\mathbf{r},\mathbf{r}',\omega)\right]\varphi_{j\tau}(\mathbf{r}')\, \varphi_{b\tau}(\mathbf{r}') \tag{3}$$

where φ are the KS orbitals and $f_{xc}^{\sigma\tau}(\mathbf{r},\mathbf{r}',\omega)$ is the exchange-correlation kernel. In this work, the kernel is approximated according to the adiabatic local density approximation (ALDA).[18]

The space spanned by the solutions of the eigenvalue equation (eq 1) corresponds to the 1h−1p excited configurations, so it is possible to approximate this space operating a selection over the configurations, keeping only those necessary for an accurate description of the phenomenon, as it is customary in ab initio CI calculations. Thus, in practice, according to the method in ref 11, the indexes which span the occupied orbital space (i and j) are limited to run only over the core shell.

KS calculations have also been performed, to evaluate the effect of configuration mixing introduced at the TDDFT level. In the KS scheme, the oscillator strength is calculated directly as the dipole transition moments between the KS one-electron eigenfunctions and the excitation energies as eigenvalue differences.

The partial density of states (PDOS) calculations have been performed in order to provide a pictorial representation of Mulliken populations related to the virtual molecular orbitals of the clusters. In particular, to find out if a given atomic function χ_μ contributes strongly to molecular orbitals at certain energies, one may weigh the different one-electron levels by using the percentage χ_μ character. If the χ_μ character is determined by the gross populations, the Gross population density of states form of the PDOS is then obtained:

$$N_\mu(E) = \sum_i \mathrm{GP}_{i,\mu} L(E - \epsilon_i) \tag{4}$$

where the index i runs over the one-electron energy levels, ϵ_i is the energy of the ith level, $L(E - \epsilon_i)$ is a Lorentzian function of 0.5 eV fwhm and $\mathrm{GP}_{i,\mu}$ is the gross population of the χ_μ function in a specific orbital density $|\phi_i(\bar{r})|^2$:

$$\mathrm{GP}_{i,\mu} = \sum_\nu P_{i,\mu\nu} S_{\mu\nu} = \sum_\nu C_{\mu i} C_{\nu i} S_{\mu\nu} \tag{5}$$

where $S_{\mu\nu}$ is the overlap matrix between the χ_μ and χ_ν basis functions and $C_{\mu i}$ are the coefficients of the χ_μ function in the ith molecular orbital (MO). In this way, $\mathrm{GP}_{i,\mu}$ is associated with the fraction of the orbital density belonging to that function (percentage χ_μ character of the MO ϕ_i).

3. Computational Details

The calculations have been performed with the ADF program (version 2003.01)[19,20] modified according to the previous section. Basis sets of the DZP type, consisting of STO functions, have been employed, recovering the experience of the previous work which has demonstrated the adequacy of the DZP basis set size if the cluster size is sufficiently large.[13] In the present work, a particular choice, the use of the frozen core (FC) computational technique, has been made in order to reduce the computing time without losing accuracy. It consists of treating explicitly only electrons in the outer levels, while the innermost atomic shells (core) are kept frozen. The following basis set scheme has been adopted on going along the series:

Mg	FC 2p	core 7s 3p/outer 2s 1p 1d
Ca	FC 3p	core 9s 5p/outer 2s 1p 2d
Sr	FC 4p	core 10s 7p 2d/outer 2s 1p 2d 1f
Ba	FC 4p	core 12s 7p 5d/outer 4s 3p 3d 1f
O	FC 1s	core 5s/outer 2s 2p 1d

An all-electron basis set is used for the excited atom which lies at the center of the cluster (see below for the cluster description).

It must be observed that the most logical freezing scheme for Ba would be FC 5p, but these calculations showed difficulties of SCF convergence, so a FC 4p scheme has been adopted analogous to the Sr basis set.

The LB94[21] exchange-correlation potential with the ground state (GS) electron configuration has been employed. It has been chosen because of its correct asymptotic behavior, which is a necessary condition for a good description of virtual orbitals. The SAOP exchange-correlation potential is also characterized by a correct asymptotic behavior, and its performance for the description of the XAS spectra has been tested in a previous work.[11] The results have been compared with the LB94 ones, showing no apparent dependency from the potentials, apart from a large shift in the absolute energy scale, due to the strong underestimate of the SAOP excitation energies with respect to the experimental values. It has been pointed out in the literature[7,22,23] that the inclusion of core hole effects in cluster calculations is essential for a good reproduction of XAS spectra, in particular for the K edge. We have tested in the previous work on MgO[13] the VWN potential[24] (which has not the correct asymptotic behavior) with the transition state configuration (TS) in order to assess the importance of core hole relaxation. We have observed some differences with respect to the LB94-GS results in the lower energy region where an increase of the pre-edge intensity is calculated in the VWN-KS scheme, in particular for the Mg K edge. However, the inclusion of response effects through the TDDFT formalism appears important for the quality of the results, in particular in the case of degenerate edges.

The exchange-correlation kernel is approximated within the usual ALDA scheme, and only excitations with singlet spin symmetry have been considered, since all the clusters have a closed shell electronic structure.

The cluster models employed for all the oxides are built extracting a proper set of atoms from the experimental cubic lattice of the NaCl type, that is fulfilled by all the oxides, using experimental M−O distances of 2.106, 2.399, 2.572, and 2.762

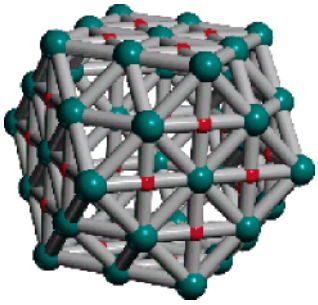

Figure 1. Cluster model $[M_{55}O_{38}]^{34+}$ employed in the present work.

Å for MgO, CaO, SrO, and BaO, respectively. The clusters have been built putting at the center the atom which is excited; successive shells of metal and oxygen atoms have been added, keeping an octahedral symmetry for computational economy. The cluster charge is chosen assuming a formal ionic configuration. This choice is related to the availability in the literature of optimized point charges (PCs) to represent the Madelung potential in cluster models for ionic systems.[25] The importance of using PCs has been already observed as decisive in our previous work on MgO oxide.[13] The final general formula adopted for the cluster with the metal atom at the center is $[M_{55}O_{38}]^{34+}$ (M = Mg, Ca, Sr, Ba) (see Figure 1) which has been embedded within an array of 250 PCs. It has to be noted that the shape of this cluster with cubo-octahedral geometry allows surface effects to be minimized due to the maximum coordination number of atoms also at the surface and appears therefore to be suitable to describe the bulk properties. The $[M_{55}O_{38}]^{34+}$ cluster has been employed for studying metal 1s and 2p thresholds. For studying the oxygen 1s threshold, we have employed the complementary $[O_{55}M_{38}]^{34-}$ cluster obtained exchanging metal and oxygen ions with each other in order to have an O atom at the origin. For this cluster, the optimized PCs are not available, so they are set to +2 and −2 for the M and O atom positions, respectively. This procedure has been previously tested,[13] giving results completely in accord with those obtained with the optimized PCs. For BaO oxide, we have been forced to use the cluster $[O_{55}M_{62}]^{14+}$ to calculate the O1s spectrum because of serious problems of convergence during SCF calculations, probably due to the large negative charge of the $[O_{55}Ba_{38}]^{34-}$ cluster.

The calculated spectra have been convoluted with Gaussian functions with a fwhm of 1.0 eV, to facilitate the comparison with the experiments.

4. Results and Discussion

In the following discussion, the calculated TDDFT spectra will be compared with the available experimental data. For this purpose, it is more convenient to consider the relative energy shifts among the features than the absolute scale; therefore, in the figures, we have shifted the experimental profiles to the calculated ones so as to make the best matches. Furthermore, to find possible trends along the series in the spectral features relative to the various core states (metal K and L edges), the calculated spectra are aligned with respect to the calculated ionization thresholds. This also allows one to have direct evidence of the spectral features lying above the ionization limit which have to be considered with caution. In this energy region, one expects to find a smooth background with some shape resonances; however, the LCAO-MO approach in a finite basis set is not capable of properly treating the continuum absorption above the edge. The effect of using a conventional basis set generates discrete states above threshold which are in part just an artifact of the calculations and represent a discretization of the nonresonant continuum. The antibonding virtual orbitals are instead closely associated with shape resonances observed in the cross section, and if the interaction with the nonresonant continuum is rather weak, it can be assumed that the high intensity discrete transitions calculated above edge may afford a qualitative estimate of the resonant features at least in the lower energy range. For these reasons, we consider the theoretical results relative to an energy range extending up to about 20 eV above the calculated ionization limit.

In the present work, we have also calculated the partial density of the unoccupied states (PDOS) of the oxides relative to each core hole analyzed. In fact, in a single particle approximation, it can be assumed that the core excitation spectrum is related to the unoccupied partial density of the states of the selected atom that is allowed by the electric dipole selection rule; therefore, we can compare it with the corresponding core excitation spectrum calculated at the KS level. The main purpose is to find a more clear interpretation of the calculated spectral features in terms of the dominant contributions of the atomic orbitals (AOs) to the final molecular orbital (MO). In fact, the nature of the excited orbitals is very difficult to characterize, in particular in big systems with a high density of states, being a mixture of many atomic components. The partial density of states can provide a pictorial representation of the Mulliken populations employing a weight factor which is related to the orbital character determined by means of a Mulliken population analysis per orbital, particularly useful when there are many one-electron levels as in cluster calculations.

4.1. Metal K-Edge Spectra. Figure 2 displays the TDDFT theoretical spectra of the metal K edge of the alkaline-earth oxides in comparison with the available experimental spectra.[3,26,27] A very low intensity is calculated for all the spectra in the region below the edge. A similar sequence of structures in the first 10 eV above the absorption edge is present in the MgO, CaO, and SrO spectra: a series of low intensity features are followed by a sharp structure at around 8 eV above edge, which dominates the spectra. This peak reproduces correctly the maximum observed in the experimental spectra of the first two oxides,[3,26,27] with the resolution of the SrO experimental spectrum being too low for making any significant comparison with the theoretical data.[28] The main deficiency of the calculations is the underestimate of the intensity of the lower energy experimental features, in both the MgO and CaO spectra, while there is a good agreement in terms of the relative energy position of the main resolved structures. At the higher energy side of the main structure, the calculations describe correctly the quite rapid intensity drops observed in the MgO spectrum and the very smooth maximum at higher energy. In the case of the CaO spectrum, a second intense peak is calculated at the higher energy side of the main peak, in accord with the large absolute maximum observed in the experiment, while the calculated intensity of the high energy part appears underestimated by the calculations. In summary, we can say that the theory is able to fairly reproduce the experimental features with a main deficiency associated with an underestimate of the intensity at lower energy. It is important to note that the discrepancy between the wider structures of the experimental profile with respect to the calculated ones does not depend on low resolution in the experiment (in the case of MgO, this is 0.5 eV and the calculated profiles are convoluted with Gaussians of 1.0 eV). The origin of this discrepancy can be associated with the coupling between the discrete orbitals and the resonant continuum, not included in the present theoretical approach as discussed before, which

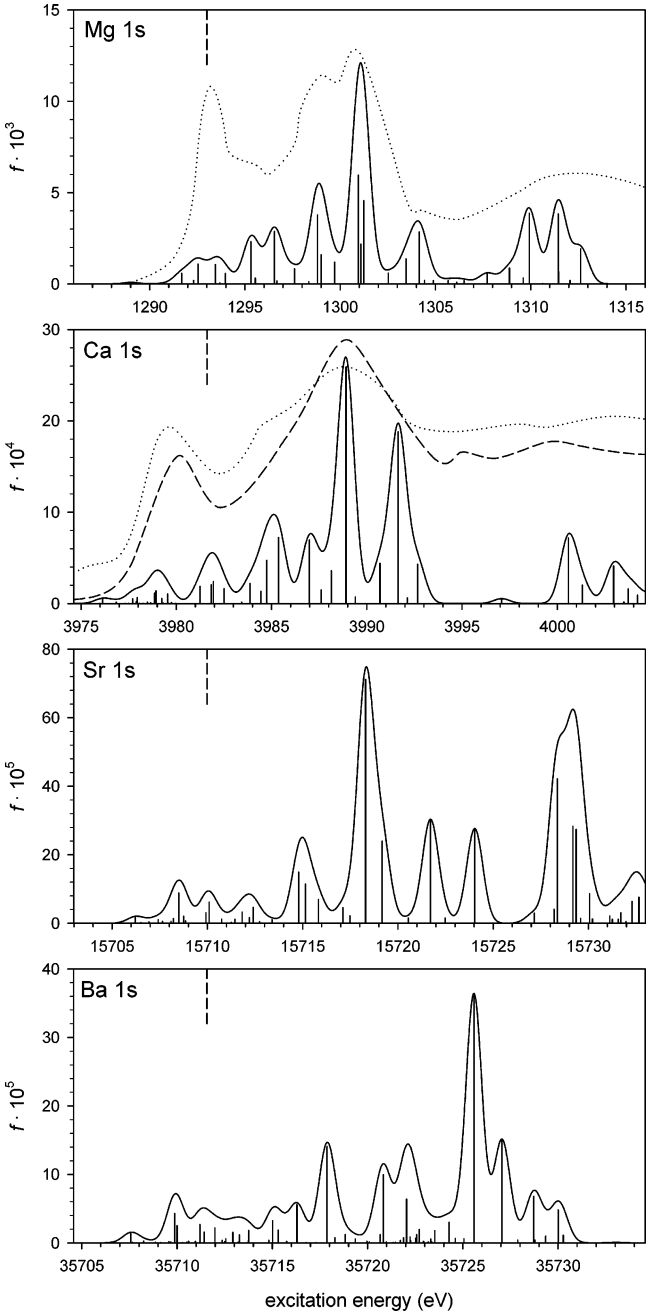

Figure 2. TDDFT metal 1s excitation spectra (solid line). Experimental data: MgO, dotted line;[3] CaO, dotted line[26] and dashed line.[27] Vertical dashed lines: calculated metal 1s DFT-KS ionization thresholds (opposite eigenvalues): MgO, 1293.01 eV; CaO, 3981.61 eV; SrO, 15 709.98 eV; BaO, 35 711.57 eV.

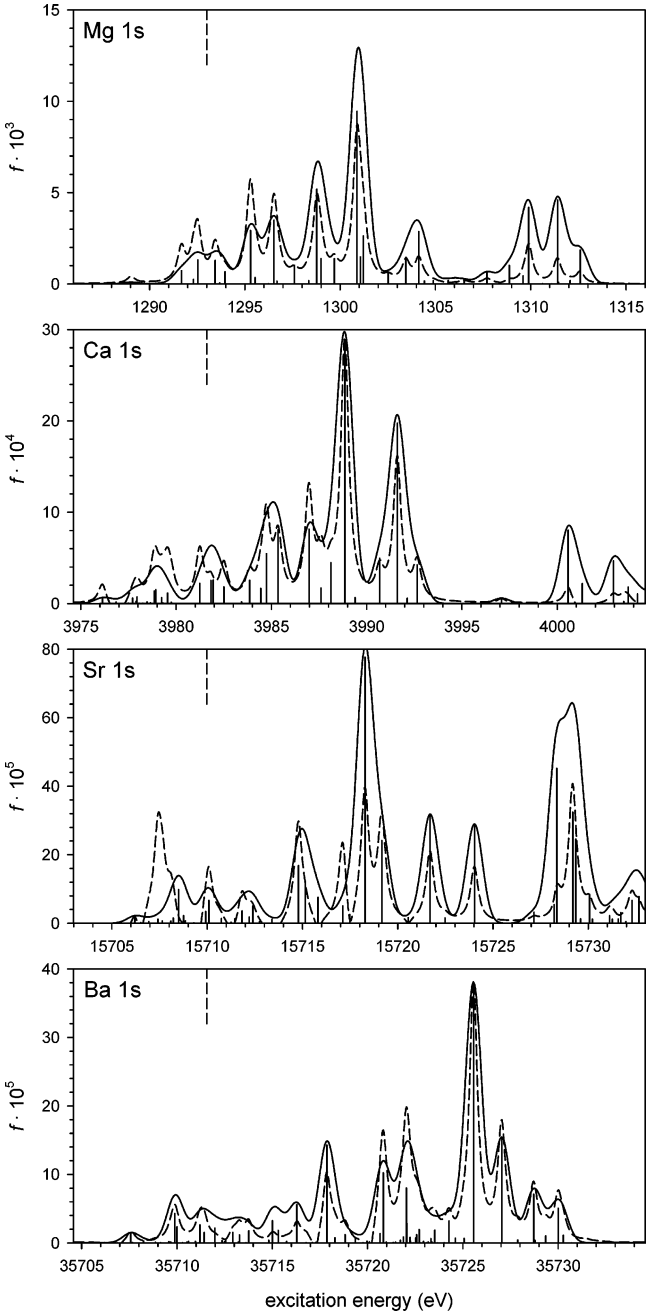

Figure 3. KS metal 1s excitation spectra (solid line) and metal p-PDOS profiles (dashed line). The DOS profiles are amplified for best fitting calculated spectra, using the following coefficients: MgO, 35; CaO, 100; SrO, 150; BaO, 130. Vertical dashed lines: calculated metal 1s DFT-KS ionization thresholds (opposite eigenvalues): MgO, 1293.01 eV; CaO, 3981.61 eV; SrO, 15 709.98 eV; BaO, 35 711.57 eV.

is responsible for the rather smooth experimental profiles observed in both the MgO and CaO spectra. Furthermore, it has to be considered as a further source of energy broadening which arises from the lifetime of the final state.[2] As concerns the calculated spectrum of the BaO oxide, a quite different spectral shape is apparent with respect to the lighter oxides. In particular, the shift of the main peak toward higher energy represents a deviation from the trend observed for the other members of the series.

To correlate the calculated spectral features with the electronic structure of the series of oxides, it is useful to analyze the theoretical results collected in Figure 3. Here, we compare the metal K-edge spectrum calculated at the one-electron KS level with the partial density of virtual states (PDOS). It has to be noted that the KS results for the metal 1s spectra are almost identical to the TDDFT ones (Figure 2), not surprisingly since the initial metal 1s orbital is not degenerate so only a small configuration mixing from the TDDFT scheme is expected. The electric dipole selection rule allows transitions from the metal 1s core orbital to the unoccupied p orbitals of the central metal atom of the cluster. The calculated oscillator strengths *f* map the contribution to the final state of the atomic orbital carrying most of the transition moment, namely, the metal np atomic components in the metal 1s excitations. The calculated PDOS of p states (p-PDOS) gives a graphical representation of the weight of the central metal p atomic character in the virtual levels; therefore, the p-PDOS can be qualitatively considered proportional to the oscillator strength calculated at the KS level. As we can see in Figure 3, there is in general a correspondence

between the p-DOS and the peaks of the KS spectra, although some discrepancies are apparent. The reported p-DOS refers to the sum of all the metal np components provided by the basis set employed. The analysis of the single np components (not reported in Figure 3) shows that the total p-DOS within about 10 eV from threshold is contributed by the lowest metal np component (namely, 3p, 4p, 5p, and 6p for MgO, CaO, SrO, and BaO, respectively). The higher np components give a not negligible contribution only in the higher energy range. As concerns the trends of the spectra along the series, a first observation concerns the significant decrease of the calculated oscillator strength *f* along the series; in particular, the intensity reduces by a factor of 5 upon going from MgO to CaO and by 1 order of magnitude upon going from CaO to BaO. This can be correlated to both initial and final state effects. The initial metal 1s orbital becomes more compact along the series, reducing the dipole overlap with the np final state and therefore the corresponding calculated *f* value. The effect of the virtual final orbitals can be instead analyzed if we consider the results of Figure 4. Here, the metal ns, np, and nd partial DOS of the $[M_{55}O_{38}]^{34+}$ clusters are reported, which allow a complete representation of these atomic contributions in the virtual levels to be obtained. The distribution of the p character in the virtual levels changes along the series. In particular, it significantly contributes to the low-lying virtual MOs of MgO while it appears strongly suppressed in CaO, where the 3d orbital becomes the major component of the Ca PDOS in the lower energy range. This situation is quite similar in SrO, where a further significant contribution from the ns components at lower energy is present while the p character contributes also to states at higher energy. This could be related to the intense peak of the KS spectrum calculated at the higher energy side of the main peak. Finally, in BaO, a general shift of the p-PDOS toward higher energy is observed which correlates with the intensity decrease around the edge and the shift of the main structures at higher energies observed in the KS spectrum. In summary, the p component carrying the most calculated transition moments is 3p in MgO, 4p in CaO, 5p in SrO, and 6p in BaO. The highest intensity peak calculated in the same energy range in the MgO, CaO, and SrO spectra is associated with the metal 1s transitions toward states dominated by these p components; also, in the case of BaO, the main peak, although shifted at higher energy, corresponds to the 1s → 6p transition. The decrease of the calculated oscillator strength along the series can be essentially associated with an increasing mixing of several AO components in the low-lying virtual states with a consequent reduction of the p character and its progressive shift toward virtual levels at higher energies.

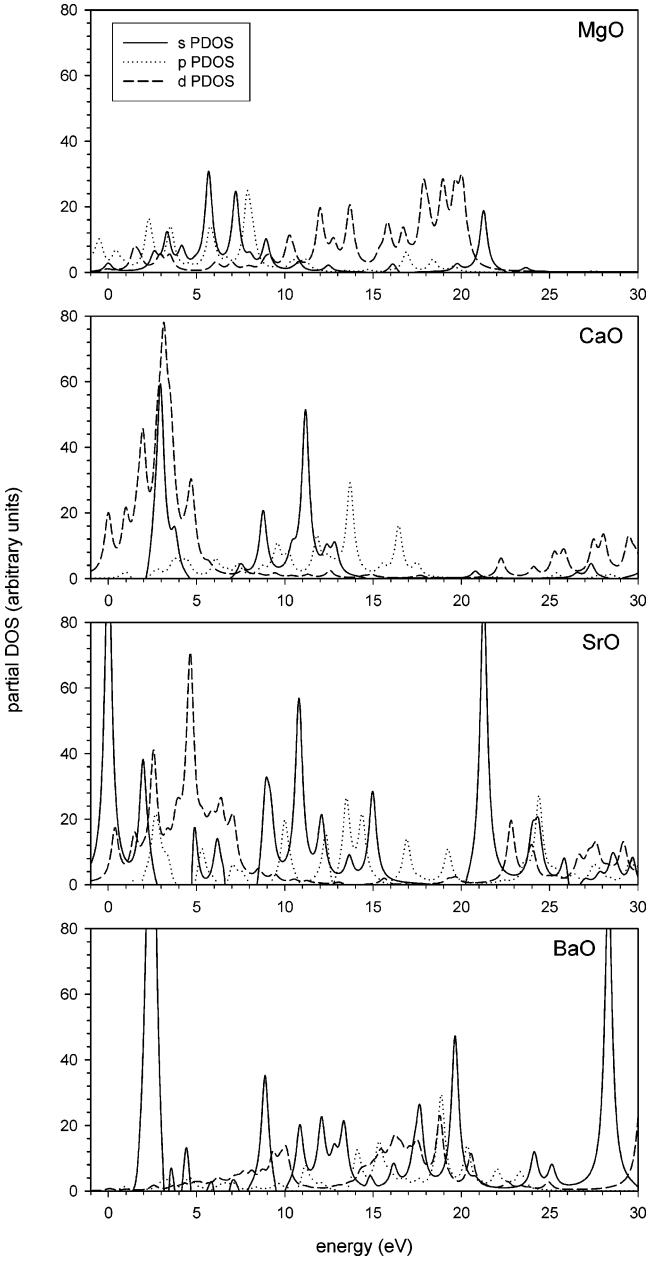

Figure 4. Partial DOS (s-, p-, and d-PDOS) profiles toward the energy of the calculated electronic levels of the cluster $[M_{55}O_{38}]^{34+}$. Energies are rescaled with respect to the LUMO KS energy value of each cluster, which is taken as zero. Absolute LUMO energies (in eV): MgO, −4.7757; CaO, −6.4548; SrO, −5.2014; BaO, −4.8624.

4.2. Metal L-Edge Spectra. The TDDFT results relative to the metal 2p excitations are reported in Figure 5 together with the available experimental data.[3,29,30] The calculated spectra show a noteworthy change in the near-edge structures upon going along the series in particular in the pre-edge region where the features strongly increase their intensity from MgO to CaO, then decrease in SrO (see the oscillator strength *f* scale in the figure), and become very low in the BaO spectrum. Also, in the case of the L edge, the BaO spectrum differs significantly from the other members of the series. The agreement between theory and experiment is nice for MgO: all the spectral structures at low energy are correctly reproduced, and also at higher energies, a general agreement is apparent, although the theoretical spectrum looks too sharp with respect to the smooth experimental profile. The CaO experimental spectrum[30] shows two very sharp structures corresponding to the $2p_{3/2}$ (L_3) and $2p_{1/2}$ (L_2) edges, which are well separated in energy. It is important to underline that the present approach does not allow the treatment of the spin−orbit effect, so it is not possible to distinguish between the L_2 and L_3 edges; therefore, the TDDFT results have to be compared with the experimental features converging to a single ionization threshold (generally Ca $2p_{3/2}$). Good agreement with the experiment in the L_3 region is found, as concerns both the energy separation and the intensity distribution of the two low energy structures. Very low intensity is instead calculated above threshold. Also, in the SrO theoretical spectrum, most of the intensity is concentrated in the structures around the edge, while, in BaO, there is a drop of the intensity at lower energy and the appearance of most important features at about 15 eV from threshold.

Consider now the calculated PDOS useful for the attribution of the calculated spectral features. The metal 2p electron has

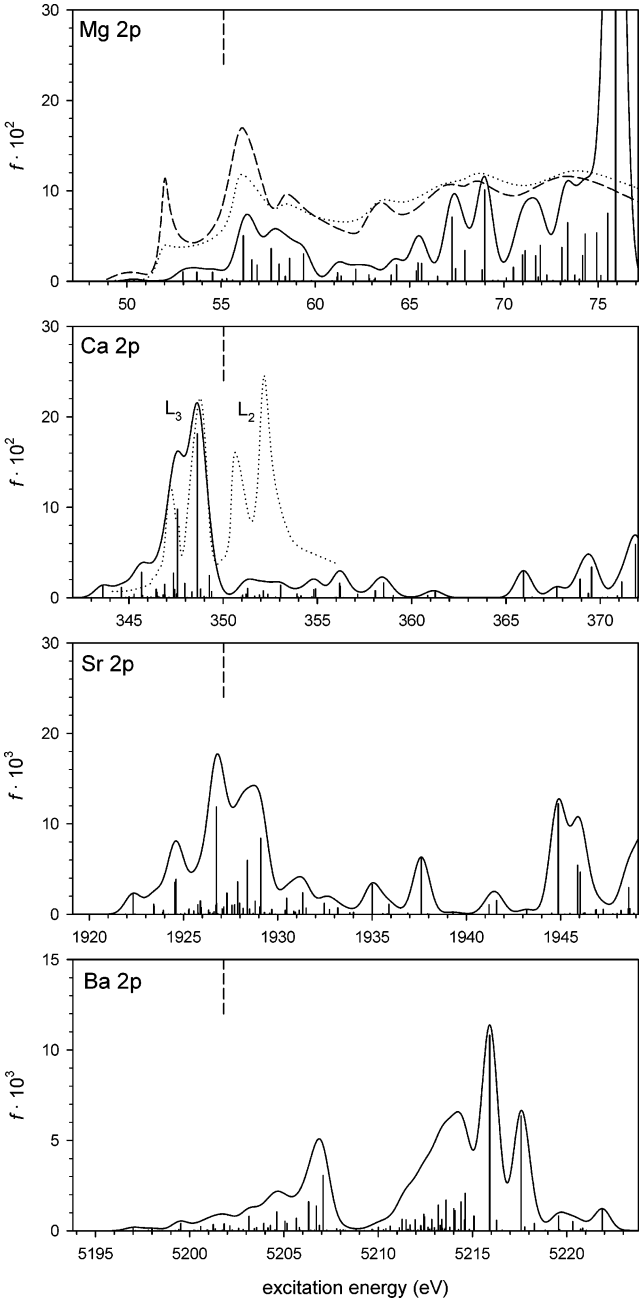

Figure 5. TDDFT metal 2p excitation spectra (solid line). Experimental data: MgO, dotted line[3] and dashed line;[29] CaO, dotted line.[30] Vertical dashed lines: calculated metal 2p DFT-KS ionization thresholds (opposite eigenvalues): MgO, 55.13 eV; CaO, 350.02 eV; SrO, 1927.12 eV; BaO, 5201.80 eV.

dipole-allowed transitions into s and d like final states; therefore, both the contributions of metal ns and nd PDOSs are considered in Figure 6, in the comparison with the theoretical spectra obtained at the KS level. A close inspection of the results reported in Figure 6 (left panel) shows that the calculated KS oscillator strengths are not properly approximated by the ns and nd contributions (we do not report their sum in the left panel). This means that the contributions of the metal ns and np components to the oscillator strengths are different, in agreement with the conclusion in the literature[31,32] regarding the different contribution of the transitions toward nd and (n + 1)s orbitals to the L-edge absorption spectra of heavier atoms. We have explicitly calculated the 2p → ns and 2p → nd oscillator strengths of the metal dications M^{2+} (M = Mg, Ca, Sr, and Ba), finding that the transitions to ns states are much less intense compared to the transitions to nd states and follow a well definite trend along the series from Mg^{2+} to Ba^{2+}. In particular, the calculated ratio between the nd and ns oscillator strengths is the smallest for Mg^{2+} (3d/3s = 11.4), while it increases significantly in Ca^{2+} (3d/4s = 62.4), Sr^{2+} (4d/5s = 51.2), and Ba^{2+} (5d/6s = 235.6). This behavior can be correlated with the more compact nature of the nd wave function with respect to the (n + 1)s wave function, resulting in a stronger overlap with the 2p wave function. In the case of the Mg dication, the 3s and 3d orbitals have the same principal quantum number, so their spatial distribution is expected to be less different, resulting in a lower ratio between the intensity of the two p−s and p−d channels. This analysis points out that the L spectrum of these oxides is dominated by the d absorption channel. If each metal ns and nd PDOS of the oxides is weighted for (multiplied by) the corresponding 2p → ns and 2p → nd computed oscillator strengths of the metal dications, the total PDOS reported in the right panel of Figure 6 is obtained. As we can see, the calculated KS oscillator strength is now found to be well approximated by the "weighted" (ns + nd) PDOSs. Figure 4 shows that in MgO the 3d orbital component dominates at higher energy and the 3s one at lower energy. In CaO and SrO, the 3d and the 4d orbitals are instead the major components of the unoccupied PDOS around the ionization threshold, although strong contributions from essentially 4s (for CaO) and 5s (for SrO) metal orbitals are also present. In BaO, the 5d component gives increasing contributions upon going toward higher energies, while the 6s component is important around threshold.

The previous investigation of the PDOS diagrams can be useful to analyze the trends of the spectral features along the series (see Figure 5). In MgO, most of the intensity around the edge is gained by the 3s virtual states and therefore the spectral features are very low. Upon going toward higher energy, the spectral intensity increases with the increase of the 3d Mg character of the final states. The high intensity of the pre-edge features of the CaO spectrum is associated with the presence of low-lying virtual states with a strong 3d metal contribution; the main s character of the higher energy states is responsible for the drop of the intensity calculated above the ionization limit. A quite similar behavior is found for the SrO spectrum, although the intensity of the transitions around the edge is lowered by about 1 order of magnitude with respect to the CaO. In fact, the maximum *f* value calculated for CaO is 0.1811, while for SrO it is 0.0119. Closely connected to this is the lower d metal (4d) character of the low-lying virtual states with respect to that found in CaO together with a less effective overlap between the 2p wave function and the 4d one with respect to the 3d wave function. Finally, the different shape of the BaO spectrum reflects the energy increase of the virtual levels with 5d metal character which give rise to intense structure far away from threshold.

It is interesting to compare the TDDFT and KS 2p metal spectra (Figures 5 and 6, respectively), to identify the role of the configuration mixing which is expected to be important in the case of the degenerate core hole, like the 2p core electrons.[33] The most significant difference between the two levels of calculations is observed in the cases of the CaO and SrO spectra: the TDDFT approach significantly redistributes the intensity of the transitions near the edge, bringing them in a better accord with the experiment in the case of CaO. Here, in particular, the mixing of the configurations tends to concentrate the intensity on two main lines (at 347.6 and 348.6 eV in Figure 5) which are associated with transitions toward final states with 3d dominant character and give rise to the two well distinct

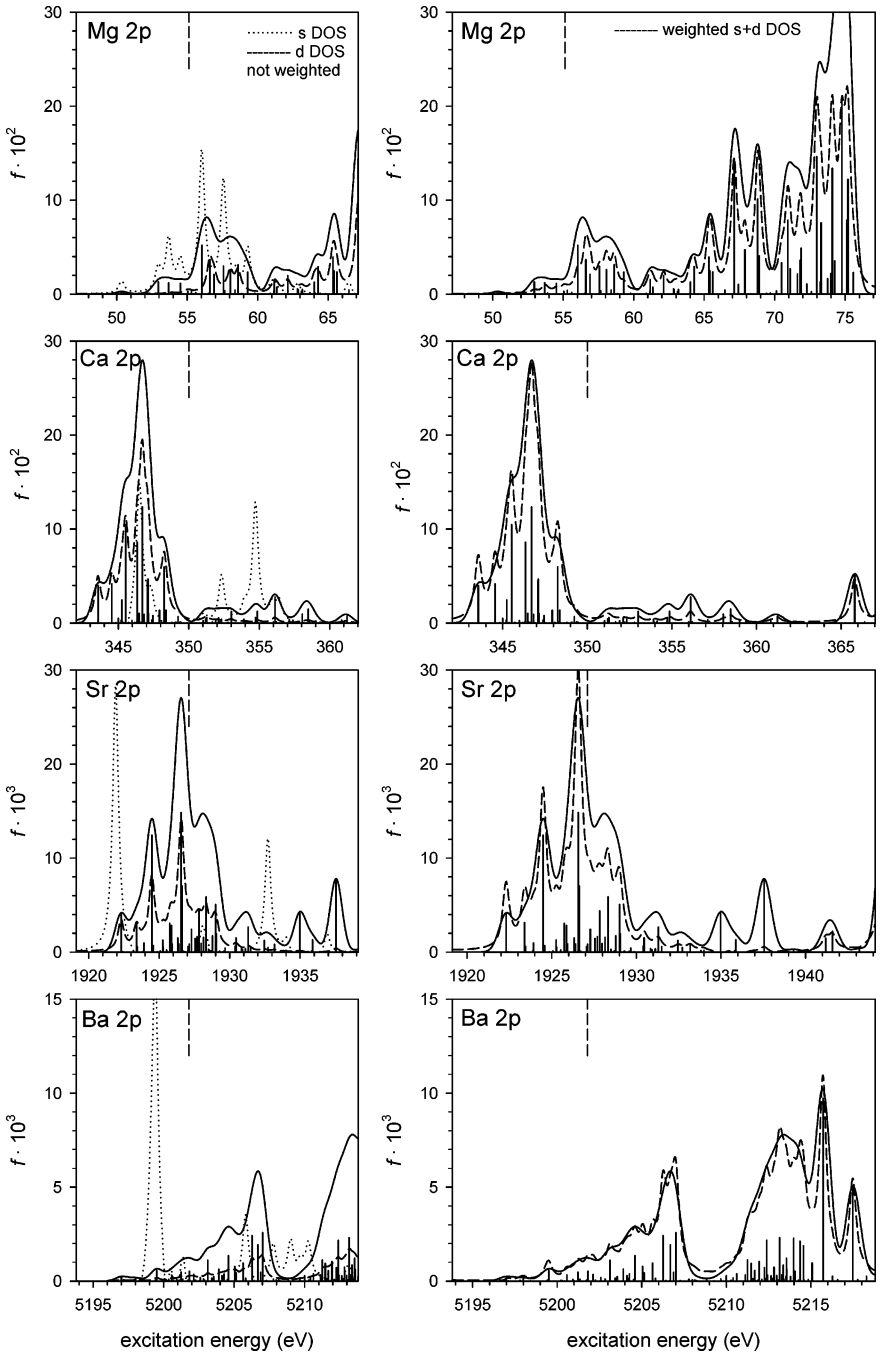

Figure 6. (left panel) KS metal 2p excitation spectra (solid line) and metal s- (dotted line) and d- (dashed line) PDOS profiles. The DOS profiles are amplified (for best fitting calculated spectra) using the following coefficients: MgO, 50; CaO, 25; SrO, 20; BaO, 10. (right panel) KS metal 2p excitation spectra (solid line) and sum of s- and d-PDOS weighted profiles; the weight coefficients are the respective 2p → ns and 2p → nd oscillator strengths relative to the calculated transitions in M^{2+} ions; the DOS profiles are reduced (for best fitting calculated spectra) using the same coefficient (2) for all the profiles. Vertical dashed lines: calculated metal 2p DFT-KS ionization thresholds (opposite eigenvalues): MgO, 55.13 eV; CaO, 350.02 eV; SrO, 1927.12 eV; BaO, 5201.80 eV.

peaks of the L_3-edge structure. Less improvement with respect to the KS results is instead obtained in the cases of the MgO and BaO TDDFT spectra, probably because the excited states at lower energies have a small d contribution. In fact, it is known that the strong configuration mixing found in the case of the 2p excitations in transition metal compounds is associated with the promotion of the 2p electron to the d valence virtual orbitals and requires an accurate theoretical treatment for a correct description of the intensity distribution.[11]

4.3. Oxygen K-Edge Spectra. The theoretical TDDFT results relative to the O K edge of the oxides are compared in Figure 7 with the experimental spectra in the same way as in previous figures. In the experiments,[3,34,35] significant changes in the near-edge structure are observed; in particular, the intensity of the first peak increases when the atomic number *Z* increases from Mg to Ca; furthermore, the shape of the first peak changes when one goes from CaO to BaO, while its energy position remains essentially the same. In the theoretical spectra, only a very small peak is calculated around 530 eV in the MgO spectrum which could correspond to the low energy shoulder of the main experimental peak, while in the other oxides this peak gains intensity and maintains its energy position (530 eV), in good accord with the experimental trend. It is important to point out that a recent theoretical work[36] on the O1s excitations in MgO

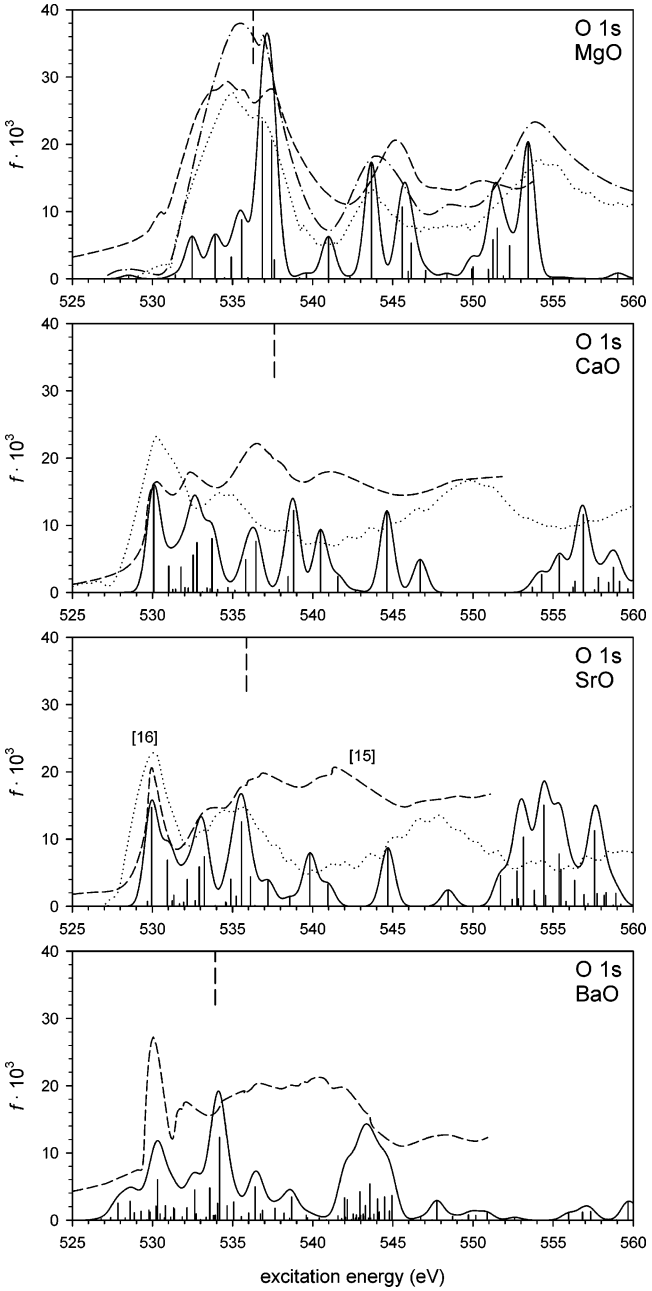

Figure 7. TDDFT oxygen 1s excitation spectra (solid line). Experimental data: MgO, dash−dotted line,[3] dashed line,[34] and dotted line;[35] CaO and SrO, dashed line[34] and dotted line;[35] BaO, dashed line.[34] Vertical dashed lines: calculated oxygen 1s DFT-KS ionization thresholds (opposite eigenvalues): MgO, 536.30 eV; CaO, 537.62 eV; SrO, 535.87 eV; BaO, 533.92 eV.

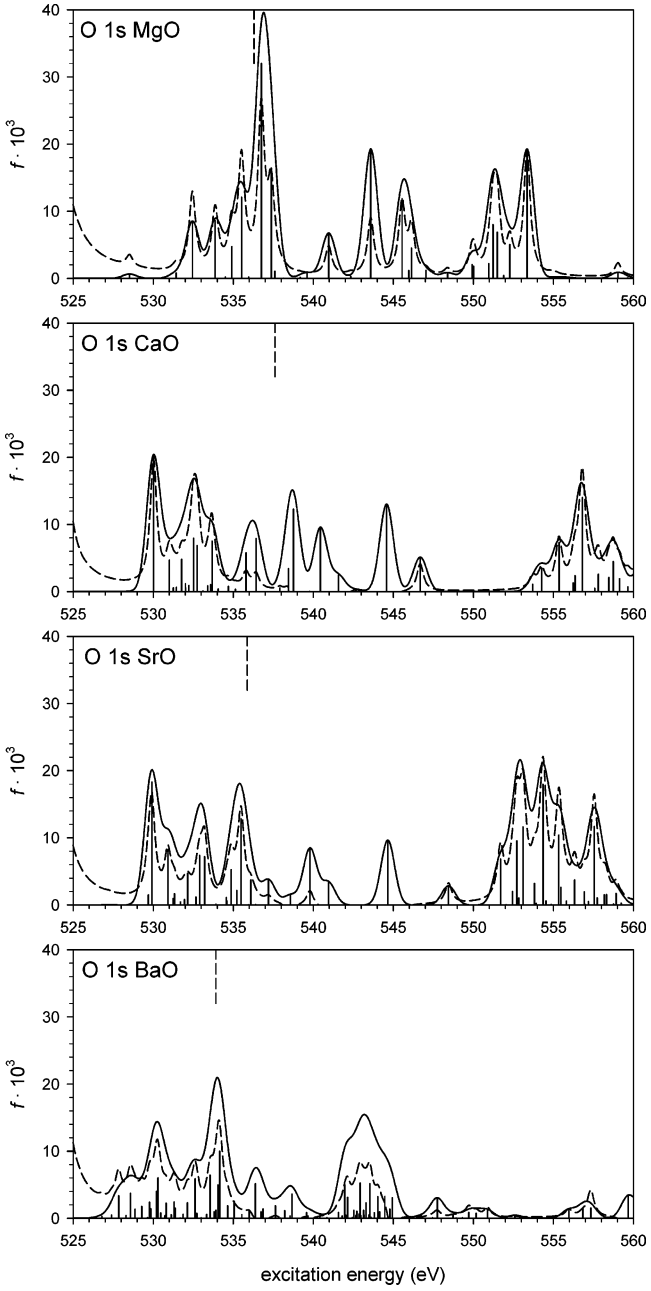

Figure 8. KS oxygen 1s excitation spectra (solid line) and oxygen p-PDOS profiles (dashed line). The latter are amplified for best fitting calculated spectra, using the coefficient 1000 for MgO and the coefficient 500 for the other profiles. Vertical dashed lines: calculated oxygen 1s DFT-KS ionization thresholds (opposite eigenvalues): MgO, 536.30 eV; CaO, 537.62 eV; SrO, 535.87 eV; BaO, 533.92 eV.

has evidenced that the small discrete peak should be ascribed to surface effects; therefore, it can be characterized by only employing surface clusters and it does not appear in calculated spectra of bulk clusters. This suggests that a complete theoretical reproduction of the O1s spectra would require the surface effects to be considered also, employing different cluster designs to simulate the bulk and the surface. Figure 7 shows that there are some discrepancies between the experimental data relative to the CaO and SrO spectra;[34,35] in particular, a different intensity trend is provided by the two experiments for both oxides in the region just above the threshold. The theoretical results resemble more closely the experimental profiles of ref 35 in this region, while a good match with both sets of experimental data is obtained for the structures calculated below the edge. For the BaO spectrum, only the experimental profile of ref 34 is available; also, in this case, the spectral features below the edge are fairly well reproduced by the calculation, while a quite different intensity distribution is apparent at higher energies. As concerns the spectral trend, a clear change of the pre-edge features upon going along the series is apparent, in particular from MgO to CaO; this change reflects the different compositions of the low-lying virtual orbitals and can be connected to the metal−oxygen interaction in these oxides. If we consider a purely ionic model for the oxide, the transitions from O(1s) to O(2p) are not allowed because the divalent oxygen ion has the 2p shell fully occupied; however, they are possible if covalent M−O interaction reduces the 2p shell occupation. In this respect, the O1s → O2p transition intensity can be a probe of the covalent character of the M−O bond, which has been proposed to increase from MgO to BaO[14] in contrast with chemical

arguments based on the electronegativity scale. The oxygen 2p character of the virtual states in the oxides can be inferred by the analysis of Figure 8, which reports the oxygen np PDOS (2p and 3p components) for the clusters centered on an oxygen atom compared with the O1s theoretical spectra at the KS level. It has to be noted that the KS results for the O1s excitations are in practice very similar to the TDDFT ones, as already observed for the metal K edges. For all the oxides, it is apparent that the below-edge structures are in agreement with the partial local density of states. We see that the O np components of the below-edge final orbitals are much lower in MgO than in the other oxides (note that the PDOS scale in MgO is amplified by a factor of 2 with respect to the other PDOS plots in Figure 8). This is consistent with the low intensity calculated for the below-edge O1s transitions of MgO, confirming the more ionic character attributed to this oxide with respect to the other members of the series. The PDOS of the CaO shows the increase of the O 2p contribution to the lowest virtual states which is responsible for the increase of the intensity calculated for the below-edge structures. The participation of the O 3p component in the low energy range is very small and becomes important only at higher energy above threshold. Analogous behavior is also observed for the oxygen np PDOS in the case of SrO and BaO; the features below edge again derive from transitions toward virtual orbitals with significant O2p contribution. In SrO, the 3p contribution is important only for the structures at high energy, as in CaO, while, in BaO, these levels are lower in energy, giving rise to the structure around 543 eV. The intensity trend of the O2p structures below the edge would therefore support the hypothesis that the ionic character is larger in MgO than in CaO, but their differences in the CaO, SrO, and BaO spectra are not so significant to represent a definite measure of the covalent mixing. It is however important to note that also the presence of the empty d levels of the metal cation are expected to play an important role in the metal−oxygen bonding interaction. Theoretical calculations[14,37] have proven that the 3d levels in MgO are too high in energy to directly participate in the bonding, while in the heaviest alkaline-earth oxides the covalent interaction is increased by the availability of metal d functions. These results agree with the intensity trend observed in the metal 2p spectra in the below-edge region previously discussed. This has been in fact associated with the presence of low-lying metal d virtual orbitals in CaO, SrO, and BaO available for direct participation in the M−O interaction. In MgO, no structures associated with 2p → 3d transitions are apparent in the spectrum in the near-edge region.

5. Conclusions

TDDFT calculations using cluster models have been performed to describe the NEXAFS absorption spectra of bulk MgO, CaO, SrO, and BaO oxides. The metal 1s and 2p edges and the O1s edge have been considered. The comparison of the theoretical results with the available experimental data shows that the present method is reliable for an affordable description of the spectra. The configuration mixing explicitly included in the TDDFT scheme appears mandatory for a correct reproduction of the oscillator strength distribution in the metal 2p spectra.

The origin of the calculated spectral features is investigated with the help of the partial density of the virtual states (PDOS) calculated for each core hole considered. The PDOS gives a graphical representation of the character of the virtual orbitals and can be qualitatively compared with the theoretical spectra calculated at the one-electron KS level.

The trend in the calculated core spectra strongly depends on the energy position of the virtual levels with nd dominant character which influences the electronic structure along the series. The cation K-edge spectra reflect the p character of the virtual states around the metal atom and therefore are not significantly influenced by the change in the nd density of states near the Fermi level and the spectra are rather similar. In the case of the 2p metal spectra, noteworthy differences are instead observed in the below-edge spectral features upon going from MgO to BaO. The trends of the below-edge features in the O1s excitation spectra are tentatively discussed in terms of the metal−oxygen bonding interaction.

References and Notes

(1) Batson, P. E. *Ultramicroscopy* **1999**, *78*, 33.

(2) Egerton, R. F. *Electron Energy-Loss Spectroscopy in the Electron Microscope*; Plenum Press: New York and London, 1996.

(3) Lindner, T.; Sauer, H.; Engel, W.; Kambe, K. *Phys. Rev. B* **1986**, *33*, 22.

(4) Bagus, P. S.; Illas, F.; Sousa, C. *J. Chem. Phys.* **1994**, *100*, 2943.

(5) Köstelmeier, S.; Elsässer, C. *Phys. Rev. B* **1999**, *60*, 14025.

(6) Sousa, C.; Illas, F.; Ricart, J. M.; Bagus, P. S. *Chem. Phys. Lett.* **1995**, *239*, 263.

(7) Mizoguchi, T.; Tanaka, I.; Yoshiya, M.; Oba, F.; Ogasawara, K.; Adachi, H. *Phys. Rev. B* **2000**, *61*, 2180.

(8) Sousa, C.; de Graaf, C.; Illas, F. *Phys. Rev. B* **2000**, *62*, 10013.

(9) Duscher, G.; Buczko, R.; Pennycook, S. J.; Pantelides, S. T. *Ultramicroscopy* **2001**, *86*, 355.

(10) Elsässer, C.; Köstlmeier, S. *Ultramicroscopy* **2001**, *86*, 325.

(11) Stener, M.; Fronzoni, G.; de Simone, M. *Chem. Phys. Lett.* **2003**, *373*, 115.

(12) Fronzoni, G.; Stener, M.; Reduce, A.; Decleva, P. *J. Phys. Chem. A* **2004**, *108*, 8467.

(13) Stener, M.; Fronzoni, G.; De Francesco, R. *Chem. Phys.* **2005**, *309*, 49.

(14) Pacchioni, G.; Sousa, C.; Illas, F.; Parmigiani, F.; Bagus, P. S. *Phys. Rev. B* **1993**, *48*, 11573.

(15) Sousa, C.; Minerva, T.; Pacchioni, G.; Bagus, P. S.; Parmigiani, F. *J. Electron Spectrosc. Relat. Phenom.* **1993**, *63*, 189.

(16) Casida, M. E. *Recent Advances in Density-Functional Methods*; World Scientific: Singapore, 1995; p 155.

(17) van Gisbergen, S. J. A.; Snijders, J. G.; Baerends, E. J. *Comput. Phys. Commun.* **1999**, *118*, 119.

(18) Gross, E. K. U.; Kohn, W. *Adv. Quantum Chem.* **1990**, *21*, 255.

(19) Baerends, E. J.; Ellis, D. E.; Roos, P. *Chem. Phys.* **1973**, *2*, 41.

(20) Fonseca Guerra, C.; Snijders, J. G.; te Velde, G.; Baerends, E. J. *Theor. Chem. Acc.* **1998**, *99*, 391.

(21) van Leeuwen, R.; Baerends, E. J. *Phys. Rev. A* **1994**, *49*, 2421.

(22) Tanaka, I.; Adachi, H. *Phys. Rev. B* **1996**, *54*, 4604.

(23) Kanda, H.; Yoshiya, M.; Oba, F.; Ogasawara, K.; Adachi H.; Tanaka, I. *Phys. Rev. B* **1998**, *58*, 9693.

(24) Vosko, S. H.; Wilk, L.; Nusair, M. *Can. J. Phys.* **1980**, *58*, 1200.

(25) Sousa, C.; Casanova, J.; Rubio, J.; Illas, F. *J. Comput. Chem.* **1993**, *14*, 680.

(26) Norman, D.; Garg, K. B.; Durham, P. J. *Solid State Commun.* **1985**, *56*, 895.

(27) Modrow, H.; Bucher, S.; Rehr J. J.; Ankudinov, A. L. *Phys. Rev. B* **2003**, *67*, 35123.

(28) Ubgade, R.; Sarode, P. R. *Phys. Status Solidi A* **1987**, *99*, 295.

(29) O'Brien, W. L.; Jia, J.; Dong, Q.-Y.; Callcott, T. A. *Phys. Rev. B* **1993**, *47*, 15482.

(30) Himpsel, F. J.; Karlsson, U. O.; McLean, A. B.; Terminello, L. J.; de Groot, M. F. M.; Abbate, M.; Fuggle, J. C.; Yarmoff, J. A.; Thole, B. T.; Sawatzky, G. A. *Phys. Rev. B* **1991**, *43*, 6899.

(31) Chaboy, J. *Solid State Commun.* **1996**, *99*, 877.

(32) Ebert, H.; Stöhr, J.; Parkin, S. S. P.; Samant, M.; Nelsson, A. *Phys. Rev. B* **1996**, *53*, 16067.

(33) Decleva, P.; Fronzoni, G.; Lisini, A.; Stener, M. *Chem. Phys.* **1994**, *186*, 1.

(34) Nakai, S.; Mitsuishi, T.; Sugawara, H.; Maezawa, H.; Matsukawa, T.; Mitani, S.; Yamasaki, K.; Fujikawa, T. *Phys. Rev. B* **1987**, *36*, 9241.

(35) Weng, X.; Rez, P. *Phys. Rev. B* **1989**, *39*, 7405.

(36) Pascual, J. L.; Pettersson, L. G. M. *Mol. Phys.* **2003**, *101*, 255.

(37) Pacchioni, G.; Bagus, P. S. *Phys. Rev. B* **1994**, *50*, 2576.